Assembly of iron phthalocyanine and pentacene molecules on a graphene monolayer grown on Ru(0001)

H. G. Zhang,[1] J. T. Sun,[1] T. Low,[2] L. Z. Zhang,[1] Y. Pan,[1] Q. Liu,[1] J. H. Mao,[1] H. T. Zhou,[1] H. M. Guo,[1] S. X. Du,[1] F. Guinea,[3] and H.-J. Gao[1,*]

[1]*Institute of Physics, Chinese Academy of Sciences, P.O. Box 603, Beijing 100190, China*

[2]*IBM Thomas J. Watson Research Center, Yorktown Heights, New York 10598, USA*

[3]*Instituto de Ciencia de Materiales de Madrid, Consejo Superior de Investigaciones Científicas, Sor Juana Inés de la Cruz 3, 28049, Madrid, Spain*

(Received 16 November 2011; published 19 December 2011)

Anisotropic triangular graphene monolayers grown on a Ru(0001) surface represent unique two-dimensional templates for creating ordered, large-scale assembly of functional molecules. Using scanning tunneling microscopy and spectroscopy, we demonstrate the selective adsorption and the formation of ordered molecular arrays of iron phthalocyanine and pentacene molecules of different structural symmetries on the graphene/Ru(0001) templates. With in-depth investigations of the molecular adsorption and assembly processes, we reveal the existence of site-specific, lateral electric dipoles (or lateral electric fields) in the epitaxial graphene monolayers and the capability of the dipoles in directing and driving the molecular adsorption and assembly. We show that the lateral dipoles originate from the inhomogeneous distribution of charge due to the epitaxial constraint of graphene on a Ru(0001) surface. The adsorption mechanism is rather general and applicable to similar molecular systems on graphene monolayers formed on other transition metal surfaces.

DOI: 10.1103/PhysRevB.84.245436 PACS number(s): 73.20.−r, 68.37.Ef, 81.16.Dn

I. INTRODUCTION

Site-specific adsorption and associated formation of ordered arrays of molecules on solid surfaces are important prerequisites for developing well-defined molecular interfaces and bottom-up molecular devices.[1,2] Over the past few decades two strategies have been mainly employed to control the adsorption and self-assembled architectures of organic molecules on well-defined surfaces. The first is to employ different molecular interactions to construct uniform molecular arrays on flat surfaces, e.g., van der Waals forces,[3] hydrogen bonding,[4] coordination bonds,[5] and covalent bonding.[6] The other way is to use nanotemplates or periodic superstructures at solid surfaces. Typical templates are Si(111)-7 × 7,[7] a Au(111) reconstruction structure,[8] an ordered moiré pattern of FeO/Pt(111),[9] and a nanomesh of h*exagonal boron nitride* (h-BN)/Rh(111).[10] Each of these templates has, however, some inherent disadvantages. Si(111)-7 × 7 surfaces are very reactive to molecules adsorbed on them, which makes diffusion, which is often necessary for the formation of ordered overlayers, all but impossible at ambient conditions, unless one uses a special class of molecules, e.g., halogenated carbon chains.[6] In some cases, the electronic and physical properties of the deposited molecules are substantially affected by the metal surface. In the case of the nanomesh template of the h-BN/Rh(111), it is isotropic. This implies that the dipole along the hole edge takes the same value along different directions, making uncertain the adsorption site and orientation of the trapped polarizable molecules. Thus, a new type of anisotropic template which does not interact with adsorbed molecules and which at the same time enables site-selective adsorption and controlled manipulations of functional molecules is highly desirable.

Recently, graphene monolayers[11,12] epitaxially grown on various metal surfaces, for example, Ru(0001),[13,14] Ir(0001),[15] Pt(111),[16] Ni(111),[17] and Cu(111),[18] have attracted great interest due to their novel properties and potential for device applications. Notably the graphene monolayers have been seen to adopt a superstructure—a moiré pattern—on some of the metal substrates. Remarkably, on Ru(0001) the graphene areas where the moiré pattern is seen reach centimeters in size, and are also stable in air and at temperatures as high as 1100 K. Thus, graphene/Ru(0001) [g/Ru(0001)] systems may be ideal templates for self-assembly of functional nanostructures[19,20] or molecules on the surfaces. Using the systems, Mao *et al.* successfully fabricated superstructures made of H_2 phthalocyanine (Pc), NiPc, and (t-bu)$_4$-ZnPc kagome lattices.[21] That work offers a tantalizing prospect of using magnetic molecules in the design of spintronic devices and the possibility of tuning the spin interaction. However, there has been very limited work exploring the fundamental physics governing molecular adsorption and assembly processes on the g/Ru(0001) surfaces and their potentials for applications in molecular device fabrications.

We report just such a combined experimental and theoretical exploration. By the use of low-temperature scanning tunneling microscopy (STM) and low-temperature scanning tunneling spectroscopy (STS) of two molecules, iron phthalocyanine (FePc) and pentacene, on epitaxially grown graphene at different growth stages, we observe the adsorption of molecules on specific sites on the g/Ru(0001) surface and the assembly of molecules into large-scale, ordered arrays. Further *ab initio* calculations reveal the existence of site-specific, lateral electric dipoles (or lateral electric fields) in the graphene monolayers and identify the dipoles as the main force in directing and driving the molecular adsorption and assembly, in contrast to the existing view that changes in the work function may be responsible.[22] Our analysis suggests that the periodic expansion and compression patterns induced by the superlattice play a role in determining the potentials at the surface, and the adsorption sites.

II. METHODS

A. Experimental details

The STM experiments were performed in an Omicron low-temperature STM system with a base pressure of 10^{-10} mbar.[23] The Ru(0001) substrate was cleaned by cycles of 1.0 keV Ar^+ sputtering followed by annealing to 1350 K, and then oxidized at about 1000 K with an oxygen pressure of 5.0 $\times 10^{-7}$ mbar for about 3 min to remove possible carbon impurities. The cleaned substrate was subsequently exposed to ethylene at 1000 K with the pressure of 5.0 $\times 10^{-7}$ mbar for about 100 s, leading to the formation of graphene/Ru(0001).[13] FePc or pentacene molecules (Aldrich, 98$^+$%) were thermally ($\sim$540 K) deposited onto the surface at room temperature (RT). Subsequently, the sample was slowly cooled down to 4.5 K in the STM stage before scanning. All voltages were applied to the sample with respect to the tip.

We chose two molecules, FePc and pentacene, as individual adsorbates for a number of reasons. FePc is among the class of tunable model molecular magnets which can take various spin configurations depending on the central metal ion and which can be potentially used in molecular spin devices. Pentacene is a typical semiconductor molecule with the potential for applications in molecular electronic devices. Moreover, while the two molecules are both polarizable, they have very different structural symmetries, a fact that can greatly facilitate our identification of the physical mechanism(s) underlying molecular adsorption.

B. Density functional theory calculation

The local density approximation (LDA) for the exchange-correlation energy, projector augmented waves (PAW), and a plane-wave basis set as implemented in the Vienna *ab initio* simulation package (VASP)[24,25] were used. The superstructure of the 12×12 graphene cells on 11×11 Ru(0001) cells is fully optimized. Recent surface x-ray diffraction (XRD) experiments have revealed a larger periodical superstructure, a (25×25) C/(23×23) Ru supercell. This supercell consists four nearly identical subcells.[26] Each subcell is quasiperiodically formed by three regions (identified below as atop, fcc, and hcp), where the electron density difference is depleted around atop and accumulated around hcp or fcc regions. Although the calculated lateral dipoles can be changed quantitatively in each subcell, the discussion in our paper would not be changed qualitatively due to the quasiperiodic hump or moiré pattern. In the following, the (12×12)C/(11×11)Ru is used instead of the whole (25×25)C/(23×23)Ru supercell. The calculated corrugation of the graphene layer in the moiré pattern along the [0001] direction is about 1.7 Å, while the minimum distance between graphene and the ruthenium substrate is about 2.2 Å, which is very close to the chemical bond length between ruthenium and carbon atoms.

Based on this configuration, we calculated the local work function and charge density. The work function is defined as the energy difference between the vacuum level and the Fermi level. In the DFT code we used, the system is periodic in the vertical direction; in this case the vacuum level is the energy at the distance from the surface where the electrostatic potential approaches a constant value. For this system a vertical height of 5.5 Å from the topmost carbon atom was used. For the calculations of molecular adsorbed system, we used the same model as that of a clean graphene/Ru(0001) system. The charge density difference of graphene/Ru(0001) was obtained by subtracting the charge density of separate graphene and Ru(0001) components from the total charge density of graphene/Ru(0001). Then the lateral dipole distribution was calculated based on this charge density difference.

III. RESULTS AND DISCUSSIONS

A. Selective adsorption of FePc molecules on g/Ru surface

Figure 1 shows the evolution of STM images of FePc molecules on the g/Ru(0001) surface with increasing molecular coverage. The g/Ru(0001) has been demonstrated to form highly ordered and long-range moiré superstructures due to the lattice mismatch between the graphene and Ru(0001).[13,26] As shown in Fig. 1(a), three different topographic features can be identified within one rhombic moiré unit cell of the superstructure, defined as "top" (triangle), "fcc" (dashed hexagon), and "hcp" (solid hexagon) regions. Such differences can be attributed to the relative location of Ru atoms at the carbon hexagon of the graphene overlayer. We observe that molecular adsorption on the g/Ru(0001) template displays unusual site specificity as the molecular coverage increases. With low molecular coverage, FePc molecules tend to occupy the fcc regions of the moiré pattern, as revealed in the STM image in Fig. 1(b). Each molecule is featured as four lobes with a bright center. With increasing coverage, FePc molecules continue to occupy more fcc regions until they form an ordered two-dimensional superlattice of isolated molecules on the graphene superstructure [Fig. 1(c)]. Once all the fcc regions are occupied, subsequent molecules prefer to adsorb at the edges of the top regions instead of adsorbing at the

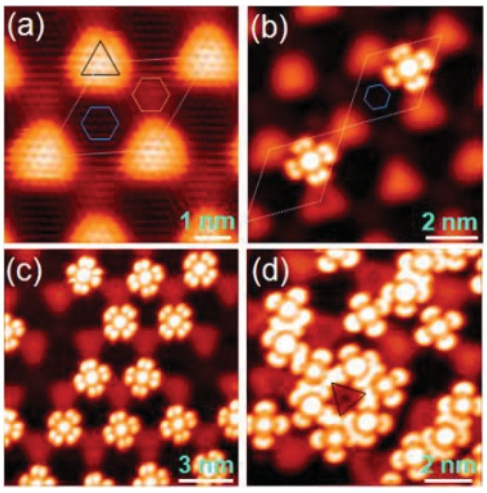

FIG. 1. (Color online) STM images of FePc molecules adsorbed on a hexagonal moiré pattern of g/Ru(0001) at varying coverage. (a) High-resolution image ($U = 0.1$ V, $I = 0.5$ nA) of three distinct regions, top, fcc, and hcp, marked by triangles and dashed and solid hexagons, respectively. (b) STM image (9 nm $\times$ 9 nm, $U = -1.5$ V, $I = 0.05$ nA) revealing that molecules first adsorb at the fcc regions. (c), (d) Sequences of STM images ($U = -2.0$ V, $I = 0.05$ nA) of FePc molecules with increasing coverage.

hcp regions. Figure 1(d) shows six molecules around the top region (drawn as a triangle) forming a hexagonal structure. The question of the responsible physical mechanisms for the observed site-specific molecular adsorption and assembly therefore arises.

Previously, the moiré pattern formed on graphene/Rh(1111) [g/Rh(111)] was employed to study the supermolecular self-assembly of perylene tetracarboxylic diimide (PTCDI). In that work, they studied the formation of different assembled structures with high molecular coverage, while the adsorption at the initial stage was not mentioned. Through comparison of the PTCDI adsorptions on the moiré pattern of g/Rh(111) to that on the nanomesh of BN/Rh(111), the authors attributed the driving force for the different assembled structures to a spatial variation of the local work function and a commensurate match between molecular dimensions and the moiré periodicity.[22] Below, we will report our systematic investigations on the molecular selective adsorption on g/Ru(0001) at the initial stage based on combining DFT calculations with the high-resolution STM data. We will first show that the mechanism based on variations of local work function does not apply to the g/Ru(0001) template. We will then reveal and discuss the physical origin of the site and orientation-selective molecular adsorption and assembly on the g/Ru(0001) template we observed.

B. Local work function on g/Ru surface

The local work function within the three regions can be determined by measuring the lateral variation of the field emission resonance (FER) and the apparent local barrier height.[27–30] It is found that higher-order peaks show a constant energy shift, corresponding to a work function variation of 0.32 eV for atop and 0.04 eV for fcc regions with respect to hcp regions [Fig. 2(a)].

To independently measure the local work function, which can also be estimated from the apparent barrier height Φ_a, we performed $I(z)$ spectroscopy. It is shown in Fig. 2(b) that the tunneling current decreases exponentially with the tip-surface distance increasing. The $I(z)$ curves in Fig. 2(b) were fitted to the simple model for the vacuum decay of the current:[31,32]

$$I(z) \propto e^{-k\sqrt{\Phi_a} z}. \quad (1)$$

Here, k is a constant depending on the units used. The local apparent barrier height Φ_a, a quantity depending directly on the local work functions, can be obtained. The values of Φ_a are 4.01, 3.80 and 3.75 eV for top, fcc, and hcp regions, respectively [inset of Fig. 2(b)]. The differences are in good agreement with the constant energy shift of the higher-order FER peaks as discussed above. These values on top and hcp regions are also consistent with the results obtained by photoemission of adsorbed xenon.[9] Although the apparent barrier height also depends on the tip work function, the spatial variation directly relates to the work function differences of the surface itself, which is especially important for capturing the subtle differences between fcc and hcp regions.

First-principles calculations based on density functional theory were used to determine the two-dimensional work function on the g/Ru(0001) surface before molecular adsorption [see Fig. 3(a)]. The calculated work functions [Fig. 3(b)] agree

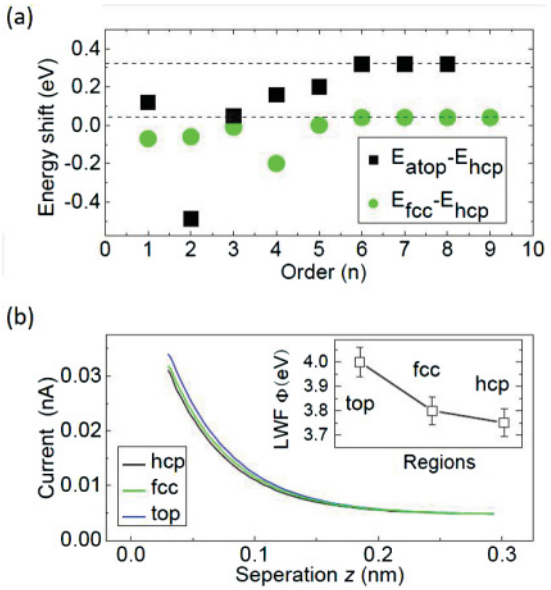

FIG. 2. (Color online) Local work function within one graphene moiré unit cell. (a) Energy shift between STS peaks of the same order as a function of the order. The peaks of the hcp region are used as the reference energies. Dashed lines mark the constant energy shifts at higher-order peaks. (b) Plots of current I vs tip-sample separation z at a constant voltage 1.0 V (initial current $I = 0.03$ nA) on three distinct regions of the g/Ru(0001) moiré unit cell. Inset shows the resulted values for local barrier height (LBH, Φ_a) by fitting to Eq. (1). The dI/dV spectra with the feedback loop on were acquired by using a lock-in technique with a 10 mV (rms) sinusoidal voltage modulation at 800 Hz. Current-distance (I-z) spectroscopy measurements were performed with the feedback loop off.

well with experimental data (Fig. 2). The top region has the highest work function, while the hcp region corresponds to the lowest one. The line profile along A to A' in Fig. 3(b) highlights the work function differences between the top, fcc, and hcp regions. The work function change correlates with desorption energies for molecules on metal surfaces, the larger the work function change, the higher the desorption energy (binding energy).[24,33,34] Therefore, we further calculate the work functions after the adsorption of FePc molecules, shown as the blue dotted line in Fig. 3(b). The work function change is found to be 0.51, 0.67, and 0.79 eV for top, fcc, and hcp, respectively, implying that the molecules would prefer the hcp regions with the highest work function change. This is clearly inconsistent with the experimental observations shown in Fig. 1, where the FePc molecules are seen to prefer the fcc regions. The calculations therefore exclude the possibility that the work function change is the guiding mechanism for the observed site and orientation specificity.

C. Lateral dipoles on g/Ru surface

To gain new and concrete insight into the mechanism underlying our experimental observation, we investigated the lateral electron density field of the g/Ru(0001) surface and its contribution to the adsorption of the FePc molecules. Figure 4(a) shows the spatial variation of the electron density difference $\Delta\rho(r)$ along two different lateral directions, top to

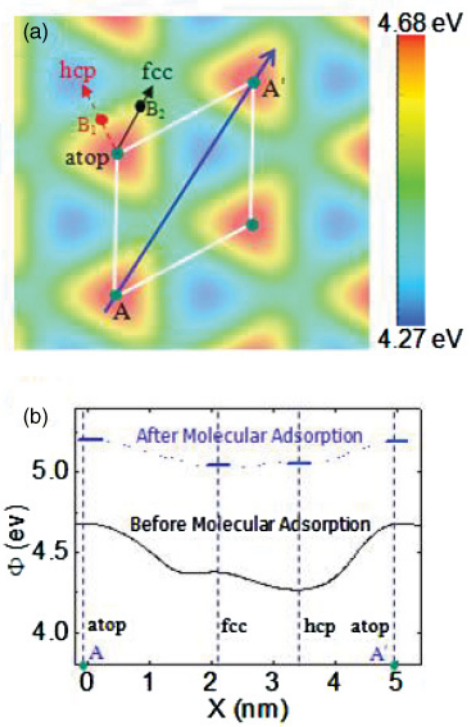

FIG. 3. (Color online) DFT calculation of local work functions of the g/Ru(0001) surface. (a) Two-dimensional map of local work functions for the fully relaxed structure of g/Ru(0001) before molecular adsorption. (b) Line profile of work functions along A to A' [marked in (a)] before (solid black line) and after (dotted blue line) molecular adsorption.

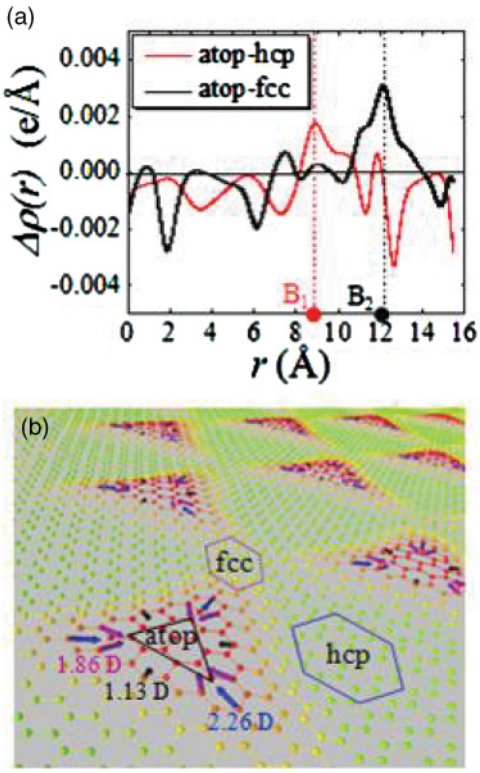

FIG. 4. (Color online) DFT calculation of lateral dipole moments on the g/Ru(0001) surface. (a) Averaged electron density difference along the top-hcp and top-fcc directions, indicated by the red dashed and black solid arrows in Fig. 3(a). Two points, B_1 and B_2, represent the boundary between the top-hcp site and top-fcc site, respectively, and are also marked in Fig. 3(a). (b) Perspective view of the inhomogeneous lateral dipole moments created by the g/Ru(0001) superstructure. Color arrows highlight different orientation and magnitudes.

hcp and top to fcc, as labeled by red dashed and black solid short arrows in Fig. 3(a), respectively. The $\Delta\rho(r)$ was defined as the difference between the electron density of the optimized g/Ru(0001) structure and the simple sum of electron densities of graphene and Ru(0001). In this calculation, the center of the top region was taken as the reference point. Comparison of two selected boundary points [B1 and B2 as shown in Fig. 3(a)] is also highlighted in Fig. 4(a). It can be seen that the distribution of the electron density difference along each of these two directions shows a significant variation that can be effectively described as a lateral electric dipole. More interesting and significant, the electron density difference at B2 is much higher than that at B1. In other words, a larger lateral dipole is expected to exist in the top-fcc direction than in top-hcp direction. This result is qualitatively consistent with our experimental observation of the preferred adsorption site, as illustrated in Fig. 1.

Lateral electric dipoles can be, and were, evaluated quantitatively with the following definition:[35]

$$\Delta\mu = \int_{r_c}^{r_c+a} (r - r_0)\Delta\rho(r)dr, \qquad (2)$$

where r_c is the position at the center of the top region, r_0 is the position of the top edge, and a is the half length of the unit cell in the lateral direction. The lateral dipoles are inhomogeneous, as seen in the perspective view in Fig. 4(b). The calculated lateral dipole moments in the top-fcc and top-hcp directions are 2.26 debye (blue arrows) and 1.13 debye (black arrows), respectively. As the FePc molecule has a large in-plane polarizability due to the metal atom at the center, these lateral dipoles create transverse electrostatic fields, whose interaction with the polarizable molecule can provide additional binding energy as in the case of a BN nanomesh.[10] At the initial, low-coverage stage of adsorption, the fcc region with the strongest lateral dipole in the top-fcc direction is energetically more favorable to the adsorbing molecules and becomes the preferential site for trapping molecules. Our calculation also shows that after the fcc regions are occupied, the slightly smaller dipoles in the top-hcp direction then kick in, leading to the trapping of molecules, again in agreement with experimental observation.

In addition we evaluate the role of the vertical dipole on the molecular adsorption, and find that the vertical dipoles are 0.404, 0.318, and 0.241 D at the center of top, fcc, and hcp regions, respectively. These dipoles are much smaller than the lateral ones. And, given their relative strength, the pattern of their spatial distributions is inconsistent with our observation of fcc as the preferred adsorption region. Thus, we conclude that the lateral dipole field and the corresponding polarization of the molecule are the dominant driving forces for the molecular assembly.

Our analysis of the lateral dipole field and its dominant role in site-specific adsorption is further supported by another

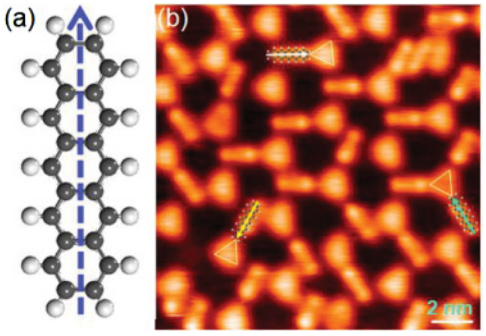

FIG. 5. (Color online) (a) Pentacene molecular structure. Blue dashed arrow is the molecular axis. (b) STM image (15.5 nm × 15.5 nm, $U = -2$ V, $I = 0.09$ nA) of the molecules adsorbed on the g/Ru(0001) surface. White triangles indicate the top regions. At low coverage the molecules adsorb preferably at the fcc region, which is consistent with what the adsorption model suggested.

controlled adsorption experiment with the second molecule of our choice, the linear-shaped pentacene, as shown in Fig. 5(a). As highlighted in Fig. 5(b), only three different kinds of molecular orientation were observed at low molecular coverage and they were all trapped in the fcc region with the molecular orientation lying along the top-fcc direction. This observation leads additional evidence supporting our conclusion that the strongest lateral dipole field on the g/Ru(0001) substrate lies in top-fcc direction. This also suggests that the control of the lateral dipole field should offer a method to control the orientation of anisotropically shaped molecules on the surface.

D. Caculation of strain effect on graphene monolayer

In fact, the existence of dipoles and other distributions of electrostatic potentials can be seen as an outcome of the inhomogeneous strain distributions induced in a superlattice unit cell. Strains modify the electronic structure and the electric charge distribution by inducing a scalar and a gauge potential.[36] To compute the strains, we assume a given height profile distribution, shown in Fig. 6(a), similar to the one calculated previously, and then relax the in-plane displacements in order to minimize the elastic energy (see supporting information[37]). Results for the induced effective magnetic field and scalar potential are shown in Figs. 6(b) and 6(c). The induced effective magnetic field varies rapidly within the unit cell, and can induce charge inhomogeneity.[36] The scalar potential, which is proportional to the local compression or dilation of the lattice, gives distinct results for the two possible absorption sites. These calculations suggest that corrugations naturally lead to strong asymmetry in the electrostatic environment between the two sites, enhancing the reactivity at selected sites. This is also in line with behavior suggested for smaller molecules.[38]

IV. CONCULSIONS

In summary, we have investigated the site- and orientation-specific adsorption and ordered assembly of functional molecules on the anisotropic triangular g/Ru(0001) templates by carrying out both low-temperature STM experiments and DFT calculations. We conclude that the lateral electric (dipole)

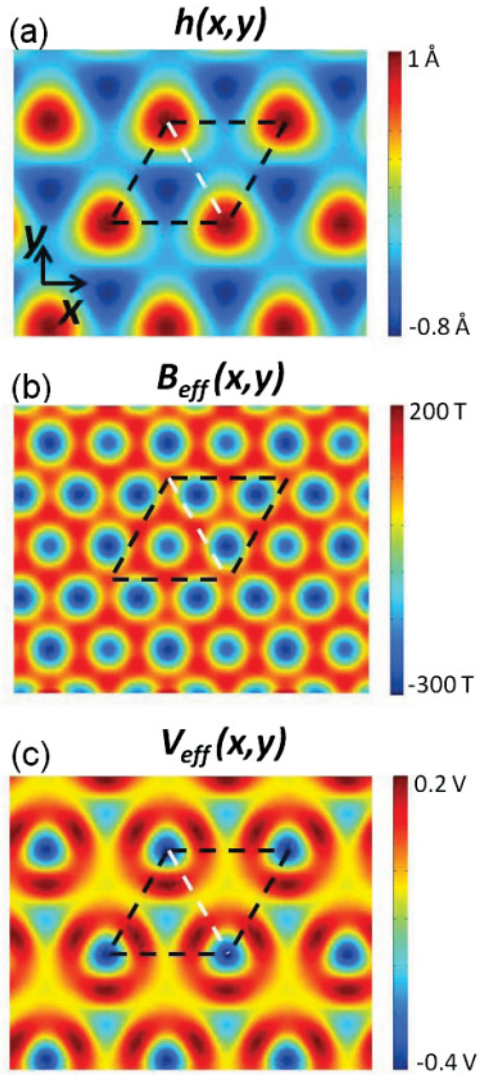

FIG. 6. (Color online) (a) Model height profile for the graphene superlattice on Ru(0001). (b) Pseudomagnetic field induced by strains. (c) Scalar potential induced by strains.

field is the main driving mechanism for "trapping" polarizable molecules into specific sites and orientations and assembling the molecules into ordered structures. Our study also suggests that the dipoles correlate well with the scalar potential induced by the corrugation of the superlattice, and the dipole-driven assembly mechanism is rather general and may be applicable to similar molecular systems on graphene monolayers formed on other transition metal surfaces and could lead to a viable route to large-scale, well-defined molecule-graphene interfaces.

ACKNOWLEDGMENTS

We are grateful to W. A. Hofer and S. J. Pennycook for critical reading of the manuscript and helpful discussions. Work at IOP was supported by grants from the National Science Foundation of China, National "973" Project of China (No. 2009CB929103, No. 2011CB932700), the Chinese Academy of Sciences, and Shanghai Supercomputing Center, China. F.G. is supported by MICINN (Spain), grants FIS2008-00124 and CONSOLIDER CSD2007-00010.

*hjgao@iphy.ac.cn

[1] H. J. Gao and L. Gao, Prog. Surf. Sci. **85**, 28 (2010).
[2] J. V. Barth, G. Costantini, and K. Kern, Nature **437**, 671 (2005).
[3] W. D. Xiao, P. Ruffieux, K. Ait-Mansour, O. Groning, K. Palotas, W. A. Hofer, P. Groning, and R. Fasel, J. Phys. Chem. B **110**, 21394 (2006).
[4] J. A. Theobald, N. S. Oxtoby, M. A. Phillips, N. R. Champness, and P. H. Beton, Nature **424**, 1029 (2003).
[5] S. Stepanow, M. Lingenfelder, A. Dmitriev, H. Spillmann, E. Delvigne, N. Lin, X. B. Deng, C. Z. Cai, J. V. Barth, and K. Kern, Nat. Mater. **3**, 229 (2004).
[6] K. R. Harikumar, T. B. Lim, I. R. Mcnab, J. C. Polanyi, L. Zotti, S. Ayissi, and W. A. Hofer, Nat. Nanotech. **3**, 222 (2008).
[7] F. Tao and G. Q. Xu, Accounts Chem. Res. **37**, 882 (2004).
[8] L. Gao, Q. Liu, Y. Y. Zhang, N. Jiang, H. G. Zhang, Z. H. Cheng, W. F. Qiu, S. X. Du, Y. Q. Liu, W. A. Hofer, and H. J. Gao, Phys. Rev. Lett. **101**, 197209 (2008).
[9] X. Lin and N. Nilius, J. Phys. Chem. C **112**, 15325 (2008).
[10] H. Dil, J. Lobo-Checa, R. Laskowski, P. Blaha, S. Berner, J. Osterwalder, and T. Greber, Science **319**, 1824 (2008).
[11] A. K. Geim and K. S. Novoselov, Nat. Mater. **6**, 183 (2007).
[12] A. H. Castro Neto, F. Guinea, N. M. R. Peres, K. S. Novoselov, and A. K. Geim, Rev. Mod. Phys. **81**, 109 (2009).
[13] Y. Pan, D. X. Shi, and H. J. Gao, Chin. Phys. **16**, 3151 (2007).
[14] S. Marchini, S. Gunther, and J. Wintterlin, Phys. Rev. B **76**, 075429 (2007).
[15] A. T. N'Diaye, S. Bleikamp, P. J. Feibelman, and T. Michely, Phys. Rev. Lett. **97**, 215501 (2006).
[16] H. Ueta, M. Saida, C. Nakai, Y. Yamada, M. Sasaki, and S. Yamamoto, Surf. Sci. **560**, 183 (2004).
[17] D. W. Goodman and J. T. Yates, J. Catal. **82**, 255 (1983).
[18] X. S. Li, W. W. Cai, J. H. An, S. Kim, J. Nah, D. X. Yang, R. Piner, A. Velamakanni, I. Jung, E. Tutuc, S. K. Banerjee, L. Colombo, and R. S. Ruoff, Science **324**, 1312 (2009).
[19] Y. Pan, M. Gao, L. Huang, F. Liu, and H. J. Gao, Appl. Phys. Lett. **95**, 093106 (2009).
[20] K. Donner and P. Jakob, J. Chem. Phys. **131**, 164701 (2009).
[21] J. H. Mao, H. G. Zhang, Y. H. Jiang, Y. Pan, M. Gao, W. D. Xiao, and H. J. Gao, J. Am. Chem. Soc. **131**, 14136 (2009).
[22] A. J. Pollard, E. W. Perkins, N. A. Smith, A. Saywell, G. Goretzki, A. G. Phillips, S. P. Argent, H. Sachdev, F. Muller, S. Hufner, S. Gsell, M. Fischer, M. Schreck, J. Osterwalder, T. Greber, S. Berner, N. R. Champness, and P. H. Beton, Angew. Chem. Int. Edit. **49**, 1794 (2010).
[23] L. Gao, W. Ji, Y. B. Hu, Z. H. Cheng, Z. T. Deng, Q. Liu, N. Jiang, X. Lin, W. Guo, S. X. Du, W. A. Hofer, X. C. Xie, and H. J. Gao, Phys. Rev. Lett. **99**, 106402 (2007).
[24] G. Kresse and J. Furthmuller, Phys. Rev. B **54**, 11169 (1996).
[25] J. P. Perdew and A. Zunger, Phys. Rev. B **23**, 5048 (1981).
[26] D. Martoccia, P. R. Willmott, T. Brugger, M. Bjorck, S. Gunther, C. M. Schleputz, A. Cervellino, S. A. Pauli, B. D. Patterson, S. Marchini, J. Wintterlin, W. Moritz, and T. Greber, Phys. Rev. Lett. **101**, 126102 (2008).
[27] R. S. Becker, J. A. Golovchenko, and B. S. Swartzentruber, Phys. Rev. Lett. **55**, 987 (1985).
[28] D. B. Dougherty, P. Maksymovych, J. Lee, and J. T. Yates, Phys. Rev. Lett. **97**, 236806 (2006).
[29] C. L. Lin, S. M. Lu, W. B. Su, H. T. Shih, B. F. Wu, Y. D. Yao, C. S. Chang, and T. T. Tsong, Phys. Rev. Lett. **99**, 216103 (2007).
[30] H. G. Zhang, H. Hu, Y. Pan, J. H. Mao, M. Gao, H. M. Guo, S. X. Du, T. Greber, and H. J. Gao, J. Phys. Condens. Mat. **22**, 302001 (2010).
[31] W. A. Hofer and A. J. Fisher, Phys. Rev. Lett. **91**, 036803 (2003).
[32] W. A. Hofer, Prog. Surf. Sci. **71**, 147 (2003).
[33] T. Livneh, Y. Lilach, and M. Asscher, J. Chem. Phys. **111**, 11138 (1999).
[34] M. L. Bocquet, A. M. Rappe, and H. L. Dai, Mol. Phys. **103**, 883 (2005).
[35] A. Michaelides, P. Hu, M. H. Lee, A. Alavi, and D. A. King, Phys. Rev. Lett. **90**, 246103 (2003).
[36] M. A. H. Vozmediano, M. I. Katsnelson, and F. Guinea, Phys. Rep. **496**, 109 (2010); F. Guinea, M. I. Katsnelson, and A. K. Geim, Nat. Phys. **6**, 30 (2010).
[37] See Supplemental Material at http://link.aps.org/supplemental/10.1103/PhysRevB.84.245436 for calculations of strain effect on selective adsorption on corrugated graphene.
[38] V. Tozzini and V. Pellegrini, e-print arXiv:1101.1178.